ELSEVIER

Journal of Neuroscience Methods 116 (2002) 15–28

JOURNAL OF NEUROSCIENCE METHODS

www.elsevier.com/locate/jneumeth

Optical imaging combined with targeted electrical recordings, microstimulation, or tracer injections

Amos Arieli [a,b,*], Amiram Grinvald [a,b]

[a] *Department of Neurobiology, The Weizmann Institute of Science, 76100 Rehovot, Israel*
[b] *The Grodetsky Center for Higher Brain Functions, The Weizmann Institute of Science, 76100 Rehovot, Israel*

Received 5 November 2001; received in revised form 30 January 2002; accepted 1 February 2002

Abstract

To facilitate the combination of optical imaging with various electrode-based techniques, we have designed and produced a skull-mounting 'sliding-top cranial window' and a removable 'electrode positioner microdrive'. These new devices were used to study sensory processing in chronic and acute experiments in the cerebral cortices of cats and monkeys. This assembly allows simultaneous optical imaging of intrinsic signals or voltage-sensitive dyes combined with extracellular recording (single and multiple unit recording and local field potential), intracellular recording, microstimulation, or targeted injection of tracers. After the functional architecture is determined by optical imaging, electrodes are targeted into a selected cortical site under full visual control, at a variety of penetration angles (30–90°), accessing a large cortical area. The device consists of three parts: (1) a skull-mounting chamber, (2) a sliding cap, and (3) a microdrive. The microdrive can easily be removed and the cranial window is then sealed and covered with a flat protective cover. For chronic experiments, this arrangement allows the animal to be handled over a long period while fitted with a sealed cranial window of minimal volume and weight, and with negligible risk of accidental damage or infection.

Keywords: Recording chamber; Sliding-top cranial window; Electrode positioner microdrive

1. Introduction

In the cerebral cortex, neurons with similar receptive fields and response properties are often clustered in columns running from the pia to the white matter (Mountcastle, 1957; Hubel and Wiesel, 1962, 1963, 1965, for review see Mountcastle, 1997). On the other hand, the tangential organization of the cortex is such that response properties undergo a gradual change, usually in a systematic manner, forming representations of the environment on the cortical surface. How the morphology and the response properties of single neurons are related to the overall functional architecture of cortical columns remains a fundamental question in neurobiology.

One effective way to study the cortex is by recording its electrical activity with microelectrodes. It is more than 40 years since the activity of a single unit in an awake behaving animal was first recorded (Hubel, 1959; Jasper et al., 1960). In these experiments the dura can be left intact, allowing the animal's brain to be maintained in good condition for periods of up to several years. A complementary technique, used to study the cortex at the level of cell populations, is optical imaging. This method has long been used to study the principles underlying cortical development, organization and function, and to process sensory information in vivo. More than 100 groups are currently using this technique (partial list: Grinvald et al., 1984, 1986, 1991; Orbach et al., 1985; Blasdel and Salama, 1986; Ts'o et al., 1990; Bonhoeffer and Grinvald, 1991; Bartfeld and Grinvald, 1992; Das and Gilbert, 1995; Godecke and Bonhoeffer, 1996; Sheth et al., 1996; Wang et al., 1996; Weliky et al., 1996; Crair et al., 1997; Rubin and Katz, 1999; Shtoyerman et al., 2000; Womelsdorf et al., 2001). In contrast to single-unit recording, optical imaging based on intrinsic signals or on voltage-sensitive dyes requires removal of the dura, so that the cortex is exposed. Recently we

* Corresponding author. Tel.: +972-8-934-3083; fax: +972-8-934-4129.
E-mail address: amos.arieli@weizmann.ac.il (A. Arieli).

0165-0270/02/$ - see front matter
PII: S0165-0270(02)00022-5

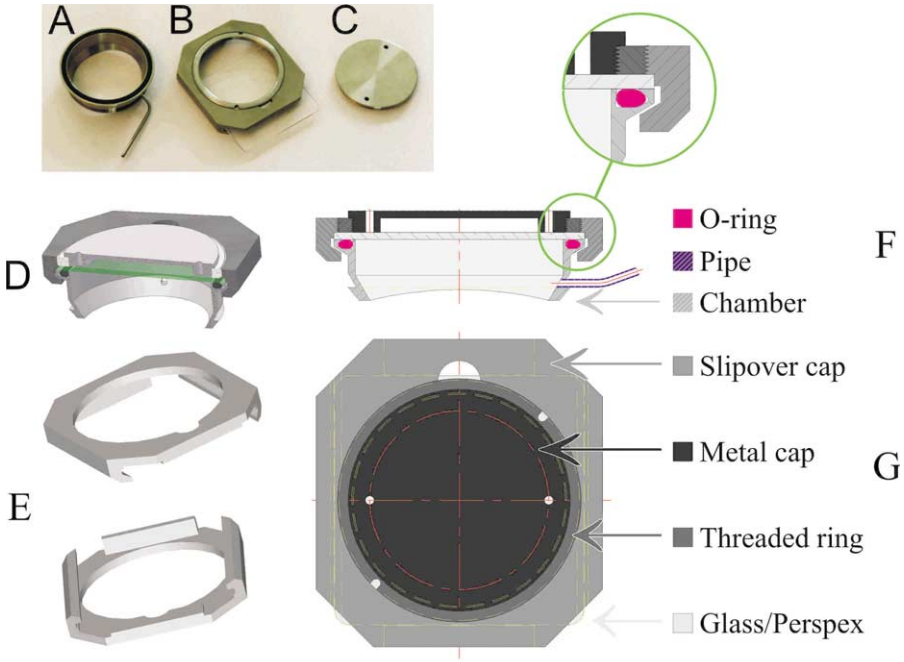

Fig. 1

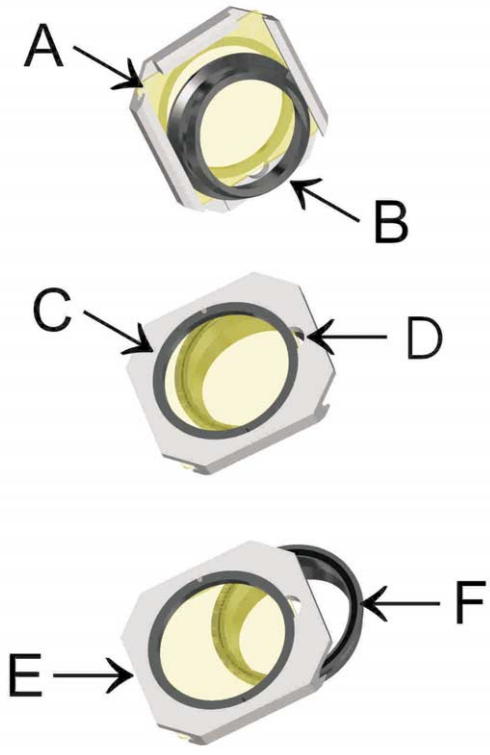

Fig. 2

Fig. 1. The sliding-top cranial window. (A) Photograph of the chamber, with an O-ring for the sliding cover. (B) Slipover cap with the Perspex cover slightly opened. A threaded ring serves as a locking nut, pressing the Perspex against the O-ring in the chamber. (C) Metal cap to protect the glass/Perspex cover when the animal is free. (D) Half-sectional view through the cranial window with all the parts assembled. (E) Two views of the slipover cap, which can move with a drawer-like action over the outer lips of the chamber. (F) Cross-sectional and top schematic view (G) of the cranial window with all its parts.

Fig. 2. Three views of the sliding-top cranial window. Bottom: the slipover cap is in its initial position. Middle and top: the window is almost closed, leaving a slit under a small opening in the upper plate, for filling the chamber before sealing. (A) Glass/Perspex; (B) chamber; (C) threaded ring (locking nut); (D) small opening to fill the cranial window while it is almost completely closed; (E) slipover cap; (F) grooved crown with O-ring.

developed a transparent silicone dural substitute, enabling optical imaging for periods longer than a year (Shtoyerman et al., 1995, 2000; Grinvald et al., 1999; Slovin et al., 1999, 2000; Arieli et al., 2002). Use of this device made it possible to combine optical imaging and the classical techniques based on microelectrodes.

The integration of optical imaging with several powerful techniques based on microelectrodes is described in this report. This integration has greatly extended the ability to tackle problems that cannot be explored by any single approach. The combined approach has enabled us, for example: (1) to confirm functional maps obtained by optical imaging; (2) to study the relationship of the morphology of the axonal and dendritic arborization of a single neuron to the cortical functional architecture; (3) to show that the network dynamics are constrained by the cortical functional architecture; (4) to examine how the dynamic state of the cortical network influences the response to a stimulus; and (5) to determine how the dynamic activity of neuronal populations over a large cortical area affects the spontaneous spike trains at the single neuron level. These and other issues can now also be addressed in relation to the behavior and the conscious state of the animal (Seidemann et al., 2000, 2002; Shtoyerman et al., 2000; Slovin et al., 2000). It is important to note that many of the techniques described here are also useful for research based on physiological recording without optical imaging. For example, they could completely change the approach to chronic electrophysiological recording in behaving monkeys, since the electrodes can be targeted into a selected cortical site under full visual control.

We describe here the details of the 'sliding-top cranial window' and the 'electrode positioner microdrive', allowing the technique to be replicated by others. We also give examples of results obtained while combining optical imaging with the various electrode-based techniques in the multiple studies mentioned above (Shmuel and Grinvald, 1996; Shoham et al., 1997; Sterkin et al., 1999; Tsodyks et al., 1999). More detailed information is available upon request. A brief report of an earlier version of the micromanipulator was published in a review (Grinvald et al., 1999).

2. Material and methods

2.1. Basic principles

2.1.1. Sliding-top cranial window

Upon exposure of the brain, required for high-resolution optical imaging experiments, two major problems are encountered: (1) movement of the brain due to heartbeat pulsation and respiration, and (2) danger of brain infection caused by contamination. In principle, these problems can be eliminated by the use of a sealed cranial window. To allow the use of microelectrodes under visual control, an electrode should be inserted through the transparent window in a way that enables it to be manipulated with a microdrive without affecting the sealing. The requirements of a chronic optical recording cranial window combined with electrode manipulation are: (1) complete sealing of the exposed cortex. The cranial window can be filled with liquid (cerebrospinal fluid (CSF)/phosphate-buffered saline (PBS) 80/20, silicon oil or agar), without any air bubbles, which would greatly interfere with optical imaging. Sealing solves the problem of brain pulsation by minimizing brain movements. Filling the cranial window to its full capacity should be possible even if the chamber is not horizontal. While opening the cranial window, large changes in fluid pressure should be avoided. (2) The inner part of the chamber should be completely smooth and easy to seal hermetically with a fully transparent cap. This solves the second major problem, that of contamination. The material in the chamber should be inert and biocompatible. Chambers with an inner thread are not ideal for maintaining the aseptic conditions needed in chronic experiments, since the thread serves as a repository for contaminating material and is difficult to clean above the exposed cortex.

None of the commercial cranial windows fulfills all of these requirements. Accordingly, we introduced two new features into the sliding-top cranial window: (1) a chamber with no inner thread (Fig. 1A, D, F, and Fig. 2B), and (2) a completely transparent slipover cap, enabling us to fill the cranial window with liquid (Fig. 1B, D–G, and Fig. 2E). The design of the cap is based on a simple mechanical principle. A glass/Perspex cover (Fig. 1B, and Fig. 2A) is pressed against an O-ring sunk into the surface of the chamber (Fig. 1A, D, F, and Fig. 2F), and slid in a drawer-like manner over the chamber's outer lips (Fig. 1D, F, and Fig. 2 bottom). The cranial window is filled and sealed as follows: the window is closed almost completely, leaving a small slit under a small opening in the upper plate (Fig. 2 top and middle). The window is filled with liquid through the opening (Fig. 2D), and the transparent cover is slid to the fully closed position. A threaded ring (Fig. 1B, Fig. 2C, locking nut) is turned, and the cap (Fig. 2E) presses the glass/Perspex cover against the O-ring, sealing it completely (Fig. 1D, F, cross-section).

2.1.2. The electrode positioner microdrive

To obtain targeted electrical recordings simultaneously with the optical imaging, we needed a removable electrode positioner microdrive that would allow: (1) a clear, wide view of the cortex; (2) easy access to a large brain area, allowing an electrode to be placed at a precise site; (3) penetration of the electrode at different

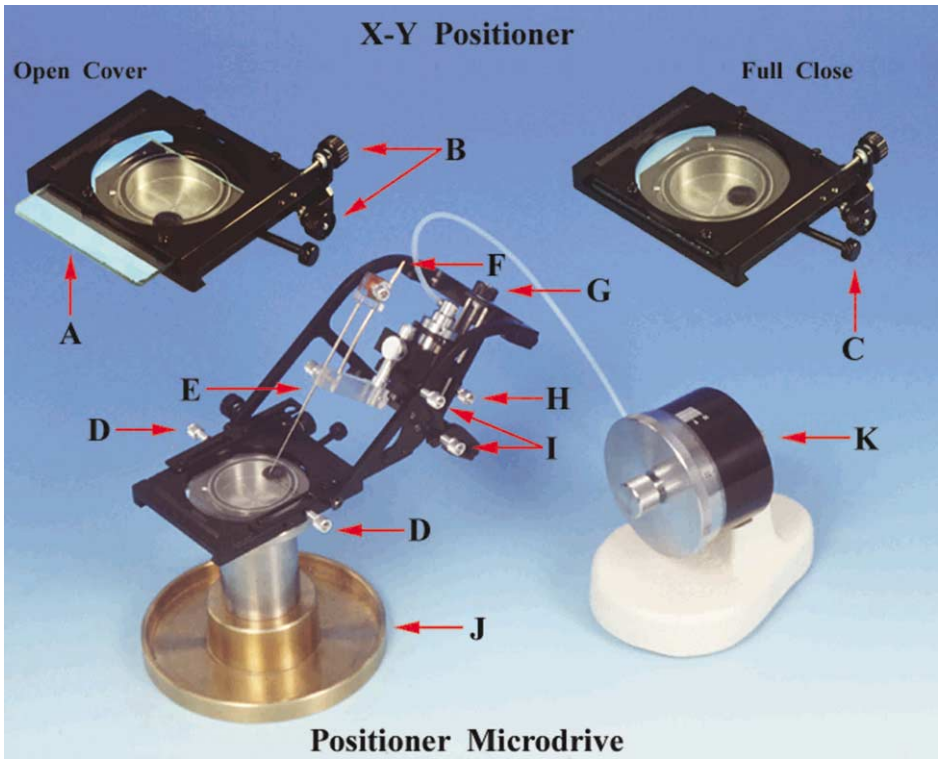
X-Y Positioner
Open Cover
Full Close
A
B
C
D
E
F
G
H
I
J
K
D
Positioner Microdrive

Fig. 3

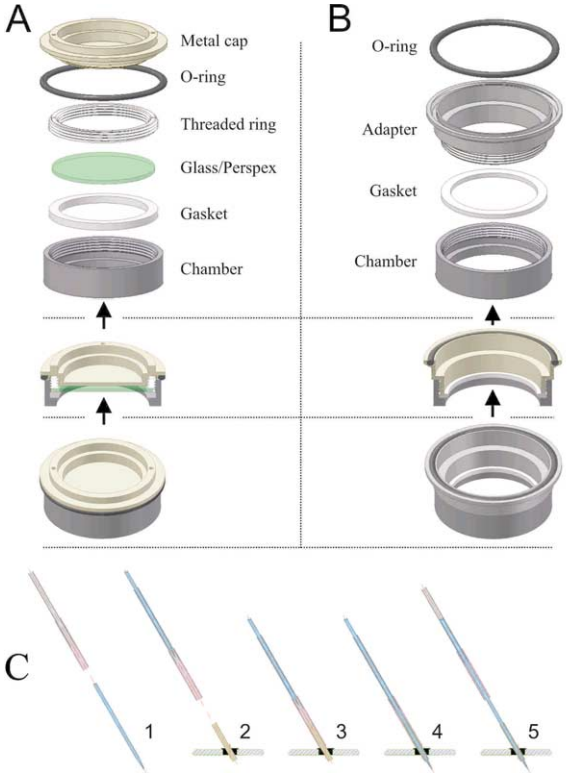
A
Metal cap
O-ring
Threaded ring
Glass/Perspex
Gasket
Chamber
B
O-ring
Adapter
Gasket
Chamber
C
1
2
3
4
5

Fig. 4

angles; (4) hermetic sealing of the cranial window and its filling to the brim (with no air bubbles), and (5) no interference with the optical apparatus. The commercially available electrode positioner microdrives are unsuitable for several reasons: (1) they do not allow a fully clear, wide view of the exposed cortex, as their upper stage is not transparent. (2) The **x**–**y** upper stage raises the surface of the chamber, causing three serious limitations: (a) disturbance of the optical apparatus: because the focal length of the lenses is short, the surface of the chamber must be close to the cortex; (b) restriction in the angle of penetration of the electrode: only an acute angle is possible. Besides the restriction itself, a sharp angle causes the electrode to collide with the lenses; (c) leakage of the liquid in the cranial window during movement of the **x**–**y** positioner microdrive to a new position; this happens because the two movement axes are located between the chamber and the electrode's penetration surface. (3) They prevent complete filling of the cranial window with liquid. (4) Penetration by the microelectrode is vertical, allowing only slight (if any) deviation of the angle.

We incorporated three design features to improve the utility of the positioner microdrive (Fig. 3 bottom). (1) The surface through which the electrode penetrates, and which moves together with the electrode holder, is a replaceable simple cover larger than the chamber, made of glass/Perspex (Fig. 3A), and is pressed and moved against the O-ring sunk into the surface of the chamber (Fig. 3 top right, 'full close'). The electrode, protected by a guide tube (Fig. 3E), penetrates the transparent surface through a rubber gasket cast onto it. (2) The transparent surface that is enclosed by the positioner microdrive, is closed by sliding it over the chamber lips in a drawer-like manner, making possible to fill the cranial window with liquid. As explained in the case of the sliding cap, this allows the user to close the transparent surface almost completely (Fig. 3 top left, 'open cover'), fill the chamber with liquid, and then slide the cover to a fully closed position. One turn of a thumbscrew, which attaches the microdrive to the chamber (Fig. 3C), presses the cover against the O-ring, sealing it completely. This arrangement raises the manipulator surface by the thickness of the 2-mm glass/Perspex cover only. The microdrive itself can move the cover, while pressed against the O-ring sunk into the chamber's surface, to any desired position (Fig. 3B). The rigid attachment of the microdrive to the chamber alone has the advantage of minimizing relative movements between the head and the microdrive and thus enhancing recording stability. (3) The electrode holder can hold an electrode at a precisely selected site at a variety of angles (30–90°; Fig. 3I).

2.2. The sliding-top cranial window—chamber and slipover cap

The 'sliding-top cranial window', a newly designed recording chamber for chronic and acute animals that can hold the microdrive, is described here (Fig. 1). The chamber is a cylinder, 8.5 mm high, made of highly polished stainless steel or titanium (Fig. 1A). To achieve a wide view of the cortex, the lower part of the chamber is conical and its upper part is cylindrical (see cross-section in Fig. 1F). An indentation on the outer surface allows the surface to be firmly gripped by dental cement. The chamber ends in a widening of the outer surface, creating a grooved crown into which an O-ring is sunk. The surface groove provides the track for the slipover cap (Fig. 1D and F), and also holds the O-ring in place when the cap is moved. To allow for sealing of the chamber, the O-ring protrudes from the upper surface of

Fig. 3. General view of the electrode positioner microdrive. Top: The **X**–**Y** positioner stage, with the glass slightly open (left) and fully closed (right). Bottom: Photograph of the positioner microdrive at an angle of $\sim 60^\circ$ on its stand. (A) Transparent sliding window (simple glass/Perspex cover) with a cast rubber gasket for insertion of an electrode protected by a guide penetration needle. (B) Thumbscrews to slide the electrode smoothly and accurately to a desired position in the **X**–**Y** plane. (C) Top right: thumb screw, which attaches the **X**–**Y** positioner to the chamber. (D) Two thumbscrews to lock the z-axis positioner to its **X**–**Y** positioner stage. (E) A 24-G stainless steel needle, which holds and protects the microelectrode, to penetrate the rubber gasket. (F) Gold pin for electrical connection with the electrode, connected to a copper plate, which is pressed against the exposed (non-insulated) part of the metal electrode. (G) Controlled coarse positioning: thumbscrew for advancing the manual manipulator along two titanium rods (a distance of 30 mm), by the rotation of a thumb worm screw. (H) Fast coarse positioning: bolt to enable or lock the rapid advancement of the hydraulic micromanipulator by sliding it manually along the same rods. (I) Two thumbscrews to lock the electrode holder at the chosen penetration angle (30–90°). (J) Stand for the positioner microdrive. (K) Commercial hydraulic micromanipulator (Narishige MO-10N), for fine movement of the electrode; travel distance up to 10 mm.

Fig. 4. (A) An alternative cranial window used for optical imaging in behaving monkeys. Bottom: Three-dimensional view of the cranial window with all its parts. Middle: Half-sectional view through the cranial window with all the parts assembled-a metal cap screwed into the cranial window on top of the breakable cover, pressing an O-ring against the surface of the inner thread, thus maintaining aseptic conditions. Top: The parts. (B) Adapter which is threaded into the chamber on one side, and to which the base of the **X**–**Y** positioner microdrive is attached on the other side. Bottom: Three-dimensional view of the cranial window with all its parts. Middle: Half-sectional view. Top: The parts. (C) Guide-pipette used for intracellular recording to prevent damage to the tip during loading. It is fitted at one end to the micropipette and at the other end to the tube in the rubber gasket through which the micropipette passes. (1) The blunt end of the pipette, covered with silicon grease, is pushed back into the wide tube of the guide-pipette (2) until the sharp tip is inside the narrow tube. (3) The guide-pipette, with the micropipette, is attached to the tube in the rubber gasket. (4) The micropipette is pushed by fingertip through the tube in the gasket. (5) The guide-pipette is pulled out. For a sharp electrode made from 1.5-mm glass tubing, the following stainless steel tubes were used: (a) a 14-G tube, in the 15-mm-long rubber gasket, protruding 10 mm above the gasket; (b) a 12-G tube, 30 mm long, and (c) a 14-G tube, 20 mm long, with an overlap of 5 mm.

the grooved crown. It is essential to prevent excision or shearing of the O-ring during movement of the slipover cap. The groove therefore contains an angled portion that holds the O-ring and keeps it in place (Fig. 1F, inset). During movement, the upper portion of the O-ring remains protruding, retaining the sealed feature of the cranial window. An important feature of the sliding-top cranial window is its ability to maintain the O-ring in place at all times, thus keeping the window sealed. The slipover cap is a square cover slip (Fig. 1B and E) that holds a glass/Perspex cover (2 mm thick), which is held in place as the cap slides with a drawer-like action over the chamber lips (see cross-section in Fig. 1D and F). Turning the threaded ring (Fig. 1B, F and G), which is screwed in the cap's upper surface on top of the glass/Perspex cover, allows complete sealing, as the O-ring is then pressed from all directions.

In the cat visual cortex, we use a single cranial window to record from both hemispheres. In order to fit the cranial window in the desired place, centered as close as possible to the skull surface and perpendicular to the cortical surface, we designed the bottom margin of the chamber as a curve (Fig. 1F). For recordings from the monkey visual cortex, however, we use two cranial windows, one on each side, and the bottom margins are flat.

2.2.1. Use of the sliding-top cranial window

During the implant operation a stereotaxic instrument holds the animal's scalp and the chamber is fixed in the desired position. The surgically implanted chamber is mounted on the skull with dental cement: The skull and the chamber are bonded into one unit by a diluted layer of dental acrylic spread over the dried and cleaned skull bone and into the indentation on the outer surface of the chamber. A thicker and more viscous structure is then firmly bonded to the dental cement, providing the necessary mechanical strength. A final layer of dental acrylic is used in order to leave a smooth surface abutting the margins of the skin. It is important to avoid heat during the polymerization, which causes the hardening, and the cement should therefore be covered with gauze soaked with saline. For acute experiments in cats and monkeys, craniotomy is performed before the cranial window is implanted. The cranial window can have an inlet and an outlet to which tubing can be attached (cut from an 18-G needle, Fig. 1F). Through the tubing different solutions, including dyes, can be applied. Should brain edema occur, it could be alleviated by application of hydrostatic pressure through the fluid-filled cranial window. For chronic experiments in monkeys, the cranial windows and the head-holder are implanted during the same operation several months before the scalp is opened (because while the monkey is in training, the head should be held still to allow the eye position to be measured). We do not introduce an inlet and an outlet in the cranial window of chronic monkeys because these structures are excellent habitats for bacterial growth.

To support and stabilize the dental-cement cap and ensure that it remains strong for several years, we attach two securely mounted cranial-implant titanium screws (YCX-01, Crist Instrument Co., Hagerstown, MD, USA) through holes drilled in the skull. A thin layer of dental cement covers the exposed scalp inside the cranial window to protect it. Several months later, when the monkey is fully trained, we remove the thin dental layer, trephine an opening in the skull, transect the dura, and insert a silicone dural substitute—all in one operation under full anesthesia (Arieli et al., 2002). Since the cranial window is large it is important to have a metal cap that can be screwed into the window on top of the breakable glass/Perspex cover, when it is not needed for recording (Fig. 1C, D, F and G). In those cases we wanted to have the option of imaging the brain by MRI, the metal we used to produce the chamber was titanium, a strong, light, highly inert substance.

The sliding-top cranial window was used mainly for acute experiments in which only one window at a time was attached. In behaving monkeys we attach a cranial window above each hemisphere as close as possible to each other. Due to the lack of space, we usually used a former type of cranial window, which has an inner thread (Grinvald et al., 1999). To prevent contaminating material from accumulating in this inner thread, and to secure the transparent cover while not recording, we designed a metal cap holding an O-ring. When the cap is screwed into the cranial window on top of the breakable cover it presses the O-ring against the surface of the inner thread, thus allowing aseptic conditions to be maintained (Fig. 4A). To use the microdrive, we use an adapter threaded into the chamber. The base of the microdrive is attached to the adapter's upper surface (Fig. 4B).

2.3. The electrode positioner microdrive

A removable positioner microdrive, which easily enables repeatable relocation and penetration of a microelectrode within the cranial window, is described here (Fig. 3 bottom). The microdrive consists of three main parts.

An 'X–Y positioner' stage attached to the grooved crown of the chamber allows the electrode to be moved to any desired position in the cranial window (Fig. 3). The positioner is constructed from three square titanium plates. The upper plate encloses a replaceable transparent glass/Perspex cover (Fig. 3A) which is larger than the chamber itself and is pressed and moved, with a drawer-like action, over an O-ring sunk into the surface of the chamber. This plate can slide (x-axis) on top of a second plate, which in turn slides (y-axis) on top of a third

plate. The two upper plates move smoothly and accurately in a saw-cut path, each advancing by rotation of a worm screw (Fig. 3B). In this way the electrode can be placed at any position in the cranial window. The second plate surrounding the chamber has an opening larger than the chamber, to allow its free movement. The base of the positioner is the third plate, which has an opening equal in size to the outer circumference of the chamber's crown. On this plate are two fixed pins and one thumbscrew, all at an angle of 120° to each other, with their conical tips pointing toward the angled portion of the outer surface of the grooved crown. As the thumbscrew is closed (Fig. 3C), it presses all three tips equally against the crown. This causes them to slide down on the crown's angled surface, thus fixing the plate rigidly to the chamber while pressing the transparent cover against the O-ring and therefore sealing it completely. In this arrangement the movement of the positioner in the x- and y-axes (which moves the Perspex together with the electrode on the surface of the chamber) can be directed to any desired angle, while all the moving parts surround the sealed cranial window.

The dimensions of the microdrive were chosen to provide maximum access of ± 10 mm to cortical areas. For a smaller cranial window diameter, or if less movement is desired; the size of the **X**–**Y** positioner can be markedly reduced.

A 'tilted z-axis positioner' allows for movement of the microelectrode over a distance of up to 40 mm along the z-axis (depth). It carries a hydraulic micromanipulator, which holds the electrode guide, and is positioned in the **X**–**Y** plane by the stage of the **X**–**Y** positioner (Fig. 3 bottom). The z-axis positioner can easily be separated from the **X**–**Y** positioner stage by opening two thumbscrews (Fig. 3D), which rigidly connect the two parts (Fig. 3 top, **X**–**Y** positioner only). The z-axis positioner directs the electrode guide at a selected angle (30–90°) towards the electrode's penetration site by using a protractor that locks the electrode holder at that angle (Fig. 3I). The electrode's penetration site is the rubber gasket (diameter 5 mm) cast into the sliding glass/Perspex cover, which moves together with the z-axis positioner. The gasket is made of polydimethylsiloxane (Silicone-585, Rhone Poulenc, Paris, France), which appears in liquid form. The electrode holder can move the electrode guide with two degrees of precision: (A) Coarse positioning, rapid movement over a distance of 30 mm, achieved by manually sliding a hydraulic micromanipulator on two titanium rods (Fig. 3H) or, for a more controlled advancement along the same rods, by rotating a thumb worm screw (Fig. 3G). (B) Fine movement, achieved by the use of a commercial hydraulic micromanipulator (e.g. Narishige MO-10N, Tokyo, Japan; Fig. 3K), which accurately moves the electrode up and down over a distance of up to 10 mm (similar to the one originally described by Evarts, 1966).

The 'electrode guide' connects the microelectrode to the micromanipulator and protects the electrode tip from breaking while penetrating the rubber gasket cast in the transparent surface (Fig. 3E, small metal tubing plus plastic part plus electrode). To insert the electrode into the electrode guide the blunt end of the microelectrode is pushed back into a 24-G stainless steel needle until the sharp tip is inside the protective tube. The insulation/glass is then removed from the blunt end of the electrode in the guide. A copper plate (with a pin for connection to the amplifier, Fig. 3F) is pressed against the exposed part of the electrode to make a good electrical contact with the electrode, and to fix the electrode in the guide, as shown in Fig. 3E. After the stainless steel needle has penetrated the rubber gasket and advanced by a few millimeters, the electrode, protected up to now by the 24-G stainless steel needle, is advanced forward outside the guide tube. Its fine tip is now ready to penetrate the cortex itself. At this point the electrode is once again locked into a fixed position relative to the guide. The fine movement required for electrical recordings is achieved using the hydraulic microdrive, which is directly coupled to the guiding tube.

For intracellular recording we use an intermediate guide-pipette to prevent damage to the tip during loading. The guide-pipette is fitted at one end to the micropipette and at the other end to a stainless steel syringe used to penetrate the rubber gasket (Fig. 4C). The blunt end of the pipette is covered with silicon grease (no. 7921, Merck, Darmstadt, Germany), and is pushed back into the wide tube of the guide-pipette until the sharp tip is protected inside the narrow tube (Fig. 4C (1 and 2)). The guide-pipette is then pushed by fingertip through the tube in the gasket (Fig. 4C (3–5)).

2.3.1. Use of the electrode positioner microdrive

The z-axis positioner is separated from the **X**–**Y** positioner stage by opening two thumbscrews (Fig. 3D). The slipover cap is removed and the microdrive is fitted into the chamber, which is filled to capacity with silicon oil (Fig. 3 top). This solves a few problems: (1) it minimizes brain pulsation and stabilizes the recording; (2) it minimizes the growth of connective tissue on the cortex (in contrast to artificial CSF, which facilitates tissue growth); (3) it prevents electrical short-circuit and reduces capacitance between the electrode and its guide.

The z-axis positioner is then rigidly connected to the **X**–**Y** positioner stage by closing two thumbscrews (Fig. 3D). A tungsten microelectrode is loaded into the microdrive via the guide tube. For simultaneous optical and electrical recording, collision of the electrode with the lens is prevented by setting the electrode holder to an angle of 45–60° (e.g. a 35-mm Pentax lens with an f-

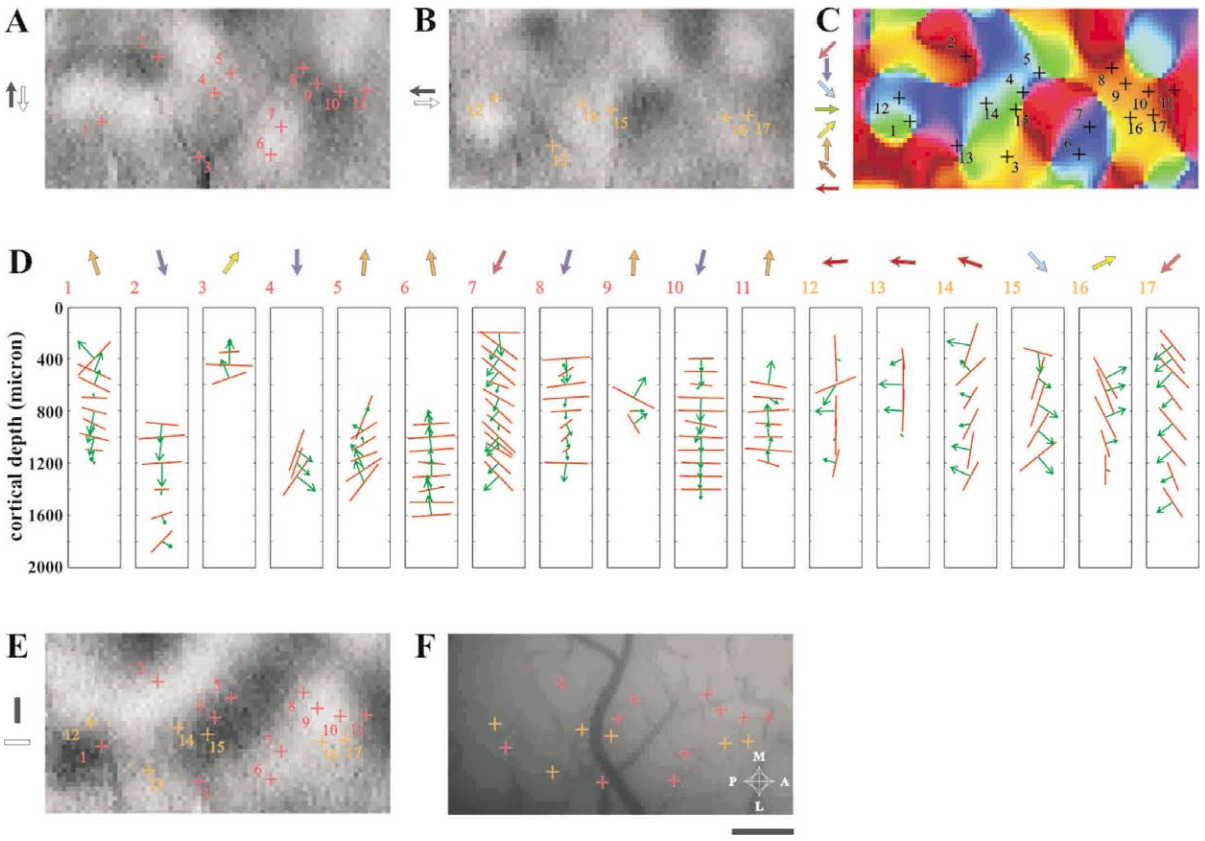
A
B
C
D
cortical depth (micron)
0
400
800
1200
1600
2000
E
I
F
M
P
A
L

Fig. 5

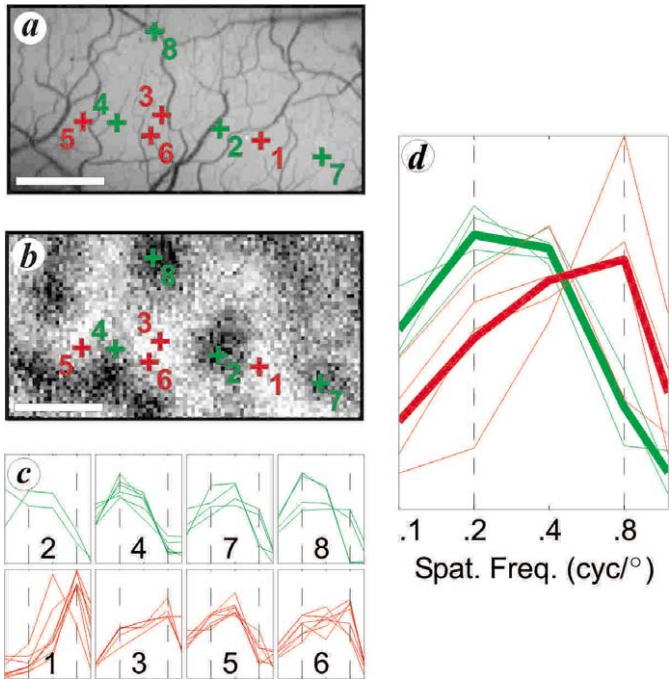
a
b
c
d
2
4
7
8
1
3
5
6
.1
.2
.4
.8
Spat. Freq. (cyc/°)

Fig. 6

number of 1.2 provides a working distance of about 50 mm in the macroscopic configuration (Ratzlaff and Grinvald, 1991)). The location of microelectrode penetration is usually determined on the basis of pre-defined functional domains obtained from previous optical imaging sessions. The microdrive provides a clear view of the exposed cortex. The cortical coordinates of each penetration are accurately determined in the following way: (1) an image of the cortical surface is obtained using green light illumination (540 nm) to emphasize the blood vessel pattern; (2) functional maps are obtained using a particular stimulus; (3) the two images (brain vasculature and functional map) are aligned and the desired recording locations are marked on the image of the cortical vasculature; (4) penetrations are targeted into the optically imaged functional domains according to the vasculature landmarks.

To begin the penetration the electrode, protected by the guide tube, is advanced manually (Fig. 3G) until it penetrates the rubber gasket in the transparent surface. Once that happens, about 5 mm of electrode is exposed beyond the end of the guide tube. The guide tube with the exposed electrode, which can be clearly seen from above, is again advanced manually until the tip of the electrode is a few millimeters from the cortex. The microelectrode is then connected via the head-stage to an amplifier and from there to an oscilloscope and audio monitor. Since the cranial window is filled with silicon oil, the measured impedance of the electrode is practically infinite, and a large, 50/60-Hz line-frequency noise is therefore seen on the oscilloscope and heard on the loudspeaker connected to the audio monitor. Fine movement is now achieved using the Narishige hydraulic microdrive (Fig. 3K). As soon as the electrode makes contact with the CSF above the cortex, there is a clear and dramatic reduction in the line-frequency noise both in the oscilloscope trace of the microelectrode and in the loudspeaker, as a result of the great reduction in the electrode's impedance to a value below 1 MΩ. When the electrode first touches the cortex and is further advanced, there might be considerable dimpling of the cortex, which could continue after penetration. This dent can cause pressure on the underlying neuronal tissue. Soon after cortical penetration there is the familiar sound of spontaneous spike activity or firing of injured neurons. After this initial stage of cortical penetration, the electrode should not be advanced any further until the dent disappears and the pressure is alleviated. When this happens the recording becomes stable, and there are no signs of cell injury or sudden loss of unit recording. If the cranial window is perfectly sealed, single-unit recordings are exceptionally stable for many hours. Intracellular recordings using a sharp micropipette are often stable for about 20 min. Due to the initial dimpling in the cortex when the electrode first penetrates, it is difficult to determine the depth of the electrode in the cortical tissue. The depth should therefore be measured again by reading the microdrive's units at the end of a penetration, while the electrode is being withdrawn. Using a tungsten microelectrode, the electrical signal is amplified and band-filtered at 300–6000 Hz (MCP1000, Alpha-Omega, Israel). It is possible to identify one or two isolated neurons using a spike sorter (MSD, Alpha-Omega, Israel), and multi-unit activity can be recorded using a window discriminator (Fredrick-Haer).

Fig. 5. Confirmation of optical maps by targeted unit recordings. (A) and (B) Differential direction maps for upward vs. downward motion and leftward vs. rightward motion, respectively. These maps were used to guide the vertical penetrations of an electrode for multi-unit recording. Crosses on both direction maps mark the locations of penetrations guided by each map. (C) Map of preferred angle of direction, computed by pixel-wise vectorial addition. (D) Results of the guided penetrations. The first 11 panels illustrate the results of penetrations guided by the direction map of upward vs. downward motion, and the last six frames illustrate those guided by the direction map of leftward vs. rightward motion. The number at the top of each individual column indicates the number of the penetration, as marked in A–C. The vertical axis of each column is scaled to the range of 0–2000 μm, representing estimated cortical depth. The preference of multi-unit for orientation (red lines) and direction (green arrows) is presented as a function of cortical depth. The lengths of lines and arrows are proportional to the normalized magnitudes of selective responses for orientation and direction, respectively. Colored arrows above the columns correspond to the preferred direction detected by optical imaging. The colors correspond to the colors of the preferred direction angle map. (E) Differential orientation map, obtained by stimulating with the grating pattern. Black and white areas represent cortical locations that preferred vertical and horizontal orientation, respectively. (F) The locations of all penetrations are marked on top of the imaged cortical area. The pattern of superficial blood vessels was used to guide the electrode to the location selected for recording. Modified from Shmuel and Grinvald (1996).

Fig. 6. Electrophysiological confirmation of the spatial frequency maps. (a) Image of the cortical surface (area 17) obtained with green light (540 nm) to emphasize the blood vessel pattern. (b) Spatial frequency domains. The differential activation map was produced by dividing the average image of 96 trials obtained with four drifting gratings of 0.2 cycle per deg (orientations of 0, 45, 90, and 135°) by the corresponding image obtained with stimuli of 0.6 cycle per deg. The temporal frequency was 2 Hz for all stimuli (similar results were obtained when the velocity was kept constant). The dark patches in the map correspond to regions that were activated more strongly by the low spatial frequency, whereas the white areas were activated more strongly by the high spatial frequency. The gray scale corresponds to a fractional change of 2.4×10^{-4} (imaging was done with red light, 707 nm). Electrode penetrations aimed at low spatial frequency domains are marked with green crosses, and those in high spatial frequency domains with red crosses. (c) Normalized tuning curves from all multi-unit recordings are shown (green for 'low' sites, red for 'high' sites). (d) Average tuning curves from all penetrations (thin lines, colors as in c), and the averages for all 'low' and all 'high' penetrations (thick lines). Modified from Shoham et al. (1997).

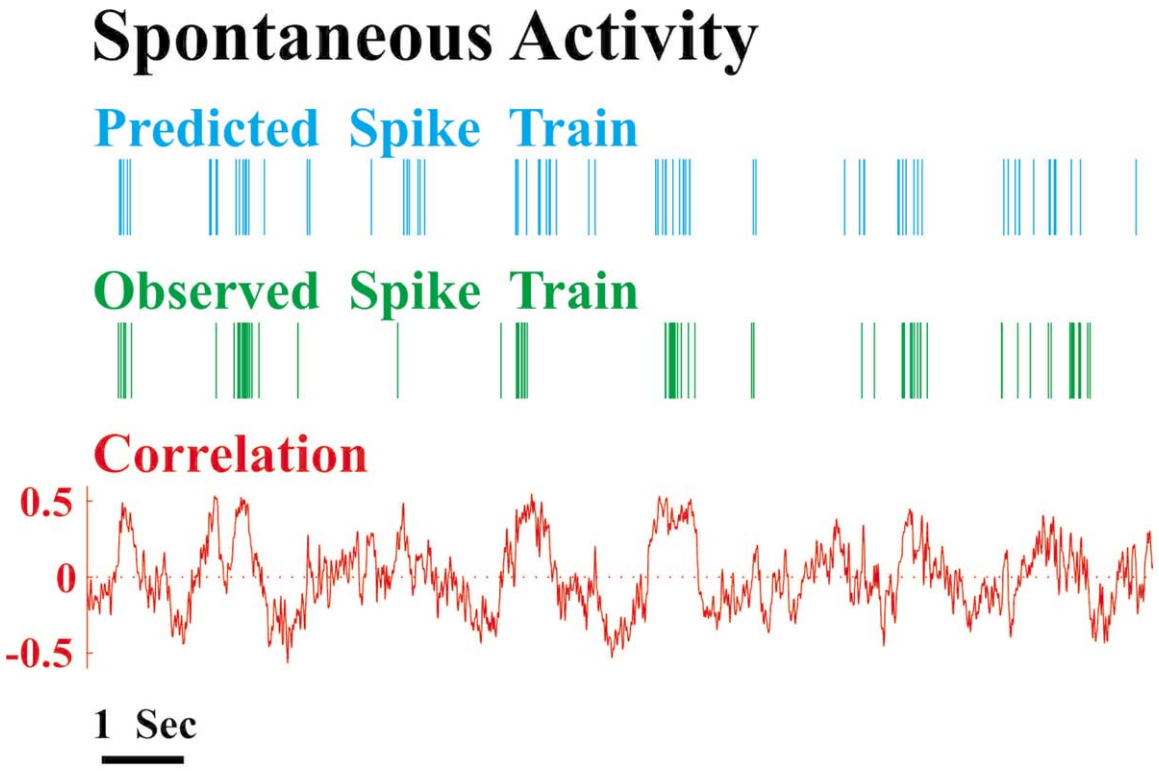
Spontaneous Activity
Predicted Spike Train
Observed Spike Train
Correlation
0.5
0
-0.5
1 Sec

Fig. 7

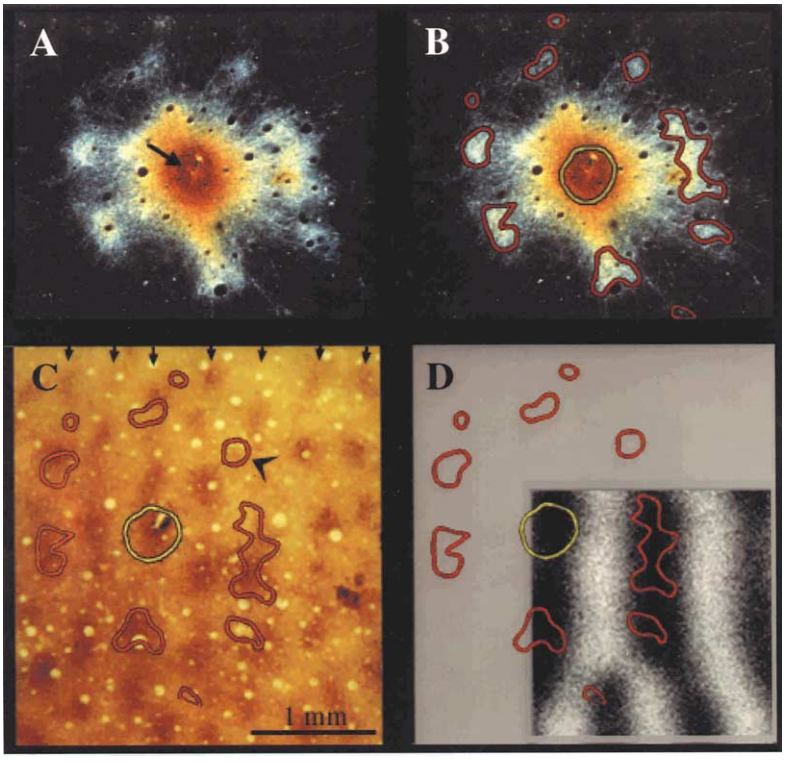
A
B
C
D
1 mm

Fig. 8

3. Results

The sliding-top cranial window with the electrode positioner microdrive for combined optical and electrophysiological recordings has been used for a number of studies in our laboratory (Shmuel and Grinvald, 1996; Shoham et al., 1997; Sterkin et al., 1999; Tsodyks et al., 1999; Shoham and Grinvald, 2001). The aim of the experiments was to record V1/V2 neurons from the visual cortex and to relate the electrical activity of single neurons to the functional anatomy and the population dynamics revealed by optical imaging. The location for microelectrode penetration was accurately determined from the relationship of the pre-defined functional maps to the cortical vascularization (see e.g. Fig. 5F and Fig. 6a). The positioner microdrive, with its wide view of the exposed cortex, was used to target the electrode into functional domains pre-defined by intrinsic signals or voltage-sensitive dyes. A Narishige hydraulic microdrive attached to the tilted z-axis positioner advanced the electrode into the cortex.

Targeted electrical recording is a useful way to address a variety of questions. For example, to confirm the columnar organization found by optical imaging in an experiment using intrinsic signals (Shmuel and Grinvald, 1996; Shoham et al., 1997), single-unit recordings were obtained separately from the imaging session by setting the electrode holder to an angle in which vertical penetration was achieved. As another example, using voltage sensitive dyes the relationship between population dynamics and single-unit activity was examined (Sterkin et al., 1999; Tsodyks et al., 1999). These two examples are briefly described below.

3.1. Confirmation of maps depicting direction of motion in cat area 18 by unit recordings

An early study suggested that the organization of direction selectivity as a function of cortical depth differs from that depicted by the classical description of cortical columns (Berman et al., 1987). In cat areas 17 and 18, direction preference in vertical tracks was usually found to be reversed at least once, either between supra- and infra-granular layers or within infra-granular layers. Along the same tracks, orientation preference usually did not change. It was therefore suggested that the functional organization for direction selectivity may differ from the classical columnar organization.

In light of these reports, a study was conducted in our laboratory to examine whether the cells in cat area 18 are clustered according to the preferred direction, and if so, to identify the features of this mapping, and to determine whether there are reversals of direction along tracks vertical to the cortex (Shmuel and Grinvald, 1996). This study demonstrated that in cat area 18, neurons are clustered according to the preferred direction. A typical recording is shown in Fig. 5. The maps of differential direction, showing upward or downward motion (Fig. 5A) and leftward or rightward motion (Fig. 5B), together with the image of the cortical surface (Fig. 5F), guided the location of the penetrations. Electrode penetrations, marked by crosses superimposed on the maps, were located close to the centers of patches selective for direction. The preferred orientation, detected by multi-unit recording along each column (as presented in Fig. 5D), was relatively constant. As with direction, most of the preferred orientations detected by electrical recording showed high correlation with those detected by optical imaging (Fig. 5E, differential orientation map). Note that the panels in which the preferred orientation of multi-units was oblique, such as columns #4, #5, #15, and #17, were located, as expected, in gray zones between the black and white patches of the orientation map. Thus, their preference for oblique orientation is consistent with the preference detected by optical imaging.

Extensive single-unit and multi-unit electrical recordings targeted to selected domains of the functional maps not only confirmed the features revealed by optical

Fig. 7. Prediction of spontaneous spike trains of a single neuron from the similarity between the functional architecture and spontaneous patterns of cortical activity. Bottom red trace: the similarity, evaluated by the correlation coefficient, between the instantaneous spatial pattern of ongoing population activity and the orientation map for the orientation tuning of the recorded neuron. Middle green trace: the observed spike train. Comparison between the observed spike train (green bars) and the time course of the correlation coefficients (red trace) shows higher correlations when the neuron is emitting spontaneous bursts of action potential. Upper blue trace: spike train predicted from the correlation values. The probability that a neuron would fire an action potential was calculated for any given value of the correlation coefficient. Using this predicted instantaneous rate, a Poisson spike train was then generated. This procedure gave a good prediction of the occurrence of bursts in the observed spike train, rather than the exact timing of single action potentials.

Fig. 8. Targeted tracer injection reveals connectivity rules. (A–D) Biocytin injection targeted at a monocular site in macaque monkey area V1. (A) Dark field photomicrograph of a tangential cortical section showing a biocytin injection (arrow) that was placed in the center of an ocular dominance column. (B) Same micrograph as A but after the main patches were delineated (red contours). The effective tracer-uptake zone, defined under high magnification viewing, is depicted by the yellow contour at the center. (C) Biocytin patches superimposed onto a neighboring section stained with cytochrome oxidase. Note that the cytochrome oxidase blobs form rows, which run from top to bottom in the figure (indicated by small arrows). The biocytin patches tend to 'skip' one row of cytochrome oxidase blobs on each side of injection. However, a few exceptions to this rule are seen (arrowhead). (D) Same injection as in A–C but superimposed on an optically imaged map of ocular dominance columns. The injection was targeted at a contralateral eye column (coded black) at the top left corner of the optically imaged area. The tendency of the biocytin patches to skip over the ipsilateral eye column (coded white) is evident. Scale bar shown in (C): 1 mm (figure modified from Malach et al., 1993).

imaging, but also did not encounter sudden reversals of direction. This finding suggests that previously reported findings of reversals in preferred direction as a function of cortical depth might relate to tracks that were not perfectly orthogonal to the cortex. These experiments also underscore the importance of targeted electrical recordings and their advantage over 'functionally blind' recordings: once the electrode is placed at the center of a functional patch, a small deviation from an angle orthogonal to the cortical surface can be tolerated while the effect of cortical depth on the tuning properties of single cells is being examined.

3.2. Confirmation of spatio-temporal frequency domains in cat visual cortex by multi-unit recordings

The positioner microdrive was also used in experiments conducted in our laboratory to confirm the maps obtained for the representation of spatial frequency domains in the cat visual cortex. Using intrinsic signals, Shoham et al. (1997) found that there are only two types of domains, with a preference for either low or high spatial frequencies (Fig. 6b). These domains were compared with those indicated by the cytochrome oxidase staining pattern in the same cortex. Domains engaged in the processing of low spatial and high temporal frequency contents of the visual scene coincide with cytochrome oxidase blobs. The quality of the maps in kittens allowed us to compare the imaging results with multi-unit recordings targeted to the centers of the spatial frequency domains in the supra-granular layers. The tuning curves of the multi-unit activity, despite their substantial width, were almost identical at different recording depths (150–1000 μm) at the same penetration locality (Fig. 6c). Tuning curves from the 'low' sites differed significantly from those from the 'high' sites (Fig. 6d), confirming the columnar arrangement of spatial frequency preferences and the optical imaging data.

3.3. Linking the spontaneous activity of single cortical neurons and the underlying functional architecture

To examine the relationship between the activity of a single neocortical neuron and the dynamics of the network in which it is embedded (Tsodyks et al., 1999), we carried out experiments, which began by revealing the orientation columns in the visual cortex. In the next stage we combined real-time optical imaging, providing temporal resolutions of 1 ms and spatial resolution of few microns, together with single-unit recording and measurement of local field potential using the positioner microdrive. We selected neurons exhibiting a relatively high rate of spontaneous activity, sharp orientation tuning preference, and robust response to optimal orientation of drifting grating. We found that the firing rate of a spontaneously active single neuron depends strongly on the ever-changing, momentary spatial pattern of ongoing population activity in a large cortical area. To determine the pattern of the evoked cortical state for which the neuron has a maximal firing rate, we calculated the average optical imaging over all patterns observed at the times corresponding to action potentials that were evoked by the optimal stimulus. The spatial patterns thus observed were of course very similar to the orientation map of the functional architecture triggered on stimulus onset. Surprisingly, the same spatial patterns of population activity were seen both when the neuron fired spontaneously and when it was driven by its optimal stimulus. We could therefore predict the spontaneous activity of single neurons by examining the similarity of the instantaneous spatial pattern of ongoing activity, and the related functional architecture, in a large patch of cortex containing millions of neurons (Fig. 7).

3.4. Targeted tracer injections

Studies of cortical organization and function can benefit greatly from the combination of optical imaging with tracer injections. Such studies should prove particularly useful in revealing the relationships of single cell morphology—all the way from the single synaptic bouton level—to the entire functional architecture of a large population of neurons in the neocortex. Optical imaging of the functional architecture provides a picture of how certain functional parameters are represented on the cortical surface. It is therefore an ideal tool for guiding the subsequent targeted tracer injections. Furthermore, by means of such integration, morphological data such as the dendritic and axonal branching of single cells can be directly correlated with the functional organization in the same piece of tissue. In an example of this application (Fig. 8), a clearly defined ocular dominance column in V1 was obtained on-line by subtracting all the frames collected when the monkey's left eye was open from the frames collected when the right eye was open. Dark patches in a differential map represent areas preferentially activated by the first stimulus, while bright patches represent areas preferentially activated by the second. To evaluate the relationship between the double set of ocular dominance columns and the laterally projecting axons, a desired location in a monocular domain was marked on the functional map and transferred automatically to the image of the cortical vasculature, which was superimposed onto the functional maps. The fine pattern of superficial blood vessels was used to target the pipette to the proper location. The biocytin tracer was iontophoretically injected to the center of the column. Neurons residing in this monocular injection site were found to connect preferentially to several distinct patches located

at the centers of the same eye columns (Malach et al., 1993).

4. Conclusions

The 'sliding-top cranial window' and its removable 'electrode positioner microdrive' described here have made it possible to integrate optical imaging with several powerful techniques based on microelectrodes. The advantage of the sliding-top cranial window is that it has a completely transparent cover, which can be moved with a drawer-like action over the chamber's outer lips, so that it can be easily and completely filled with liquid, and the cover can then be slid over it so that the chamber is completely closed. The main achievement of the positioner microdrive is to facilitate the insertion of microelectrodes into any selected cortical site, under full visual control, after the functional architecture has been previously determined by optical imaging, or determined concomitantly by imaging with voltage-sensitive dyes. Our experiments show that the method is highly reliable, and results in the accurate placement of the microelectrode into the selected cortical site, which coincides with the expected electrophysiological signature of the functional architecture.

This assembly has extended the abilities of all of these approaches to investigate problems, both in acute and in chronic preparations, that cannot be adequately studied by any of the techniques on their own. The combined approach was used in the following studies: confirmation of functional maps obtained by optical imaging; examination of the relationship of the morphology of the axonal and dendritic arborization of single neuron to the cortical functional architecture; determination of how the network dynamics are constrained by the cortical functional architecture; investigation of how the dynamic state of the cortical network influences the response to a stimulus; determining how the dynamic activity of a neuronal population over a large cortical area affects the spontaneous spike trains at the single neuron level; exploring the specificity of the spread of electrical activity evoked by microstimulation (Seidemann et al., 2002), etc. These and other questions can now be explored by studying the behavior of awake behaving monkeys performing higher brain functions.

Acknowledgements

We thank the Instrument Design Unit of the Weizmann Institute, and especially Jehoshua Wolowelsky, Nurit Gideon, Benjamin Pasmantirer, and Lilia Goffer, for their major contribution in planning the cranial window and the microdrive. Special thanks are due to Abraham Inhoren and Dado Binyamin from the Instrument Workshop of the Weizmann Institute. We thank Rina Hildesgeim, Tal Kenet, Amir Shmuel, and Doron Shoham for participating in the experiments. Many thanks to Shirley Smith for the excellent scientific editing. This work was supported by the Grodetsky Center for Higher Brain Functions, a grant from MOS/BMBF, and the family foundations of Margaret M. Enoch, Goldsmith and Glasberg families and the Koerber Foundations.

References

Arieli A, Grinvald A, Slovin H. Dural substitute for long-term imaging of cortical activity in behaving monkeys and its clinical implications. J Neurosci Methods, 2002;114:119–33.

Bartfeld E, Grinvald A. Relationship between orientation preference pinwheels, cytochrome oxidase blobs and ocular dominance columns in primate striate cortex. Proc Natl Acad Sci USA 1992;89:11905–9.

Berman NEJ, Wilkes ME, Payne BR. Organization of orientation and direction selectivity in areas 17 and 18 of cat cerebral cortex. J Neurophysiol 1987;58:676–99.

Blasdel GG, Salama G. Voltage-sensitive dyes reveal a modular organization in monkey striate cortex. Nature 1986;321:579–85.

Bonhoeffer T, Grinvald A. Iso-orientation domains in cat visual cortex are arranged in pinwheel like patterns. Nature 1991;353:429–31.

Crair MC, Ruthazer ES, Gillespie DC, Stryker MP. Relationship between the ocular dominance and orientation maps in visual cortex of monocularly deprived cats. Neuron 1997;19:307–18.

Das A, Gilbert CD. Long-range horizontal connections and their role in cortical reorganization revealed by optical recording of cat primary visual cortex. Nature 1995;375:780–4.

Evarts EV. Methods for recording activity of individual neurons in moving animals. In: Rushmep RF, editor. Methods in Medical Research. Chicago: Year Book Medical Publishers, 1966:241–50.

Godecke I, Bonhoeffer T. Development of identical orientation maps for 2 eyes without common visual experience. Nature 1996;379:251–4.

Grinvald A, Anglister L, Freeman JA, Hildesheim R, Manker A. Real-time optical imaging of naturally evoked electrical activity in intact frog brain. Nature 1984;308:848–50.

Grinvald A, Lieke E, Frostig RD, Gilbert CD, Wiesel TN. Functional architecture of cortex revealed by optical imaging of intrinsic signals. Nature 1986;324:361–4.

Grinvald A, Frostig RD, Siegel RM, Bartfeld E. High resolution optical imaging of neuronal activity in awake monkey. Proc Natl Acad Sci USA 1991;88:11559–63.

Grinvald A, Shoham D, Shmuel A, Glaser D, Vanzetta I, Shtoyerman E, Slovin H, Wijnbergen C, Hildesheim R, Arieli A. In-vivo optical imaging of cortical architecture and dynamics. In: Windhorst U, Johansson H, editors. Modern Techniques in Neuroscience Research. Berlin: Springer, 1999:893–969.

Hubel DH. Single unit activity in striate cortex of unrestrained cats. J Physiol (London) 1959;147:226–38.

Hubel DH, Wiesel TN. Receptive fields, binocular interaction and functional architecture in the cat's visual cortex. J Physiol 1962;160:106–54.

Hubel DH, Wiesel TN. Shape and arrangement of columns in cat's striate cortex. J Physiol (London) 1963;165:559–68.

Hubel DH, Wiesel TN. Receptive fields and functional architecture in two non-striate visual areas (18 and 19) of the cat. J Neurophysiol 1965;28:229–89.

Jasper H, Ricci GF, Doane B. Microelectrode analysis of cortical cell discharge during avoidance conditioning in the monkey. Electroencephalogr Clin Neurophysiol (Suppl) 1960;13:137–55.

Malach R, Amir Y, Harel M, Grinvald A. Relationship between intrinsic connections and functional architecture revealed by optical imaging and in-vivo targeted biocytin injections in primate striate cortex. Proc Natl Acad Sci USA 1993;90:10469–73.

Mountcastle VB. Modality and topographic properties of single neurons of cat's somatic sensory cortex. J Neurophysiol 1957;20:408–34.

Mountcastle VB. The columnar organization of neocortex. Brain 1997;120:701–22.

Orbach HS, Cohen LB, Grinvald A. Optical mapping of electrical activity in rat somatosensory and visual cortex. J Neurosci 1985;5:1886–95.

Ratzlaff EH, Grinvald A. A tandem-lens epifluorescence macroscope: Hundred-fold brightness advantage for wide-field imaging. J Neurosci Methods 1991;36:127–37.

Rubin BD, Katz LC. Optical imaging of odorant representations in the mammalian olfactory bulb. Neuron 1999;23:499–511.

Seidemann E, Slovin H, Arieli A, Grinvald A. Cortical activity evoked by electrical microstimulation in visual and frontal cortical areas of behaving monkeys imaged using voltage sensitive dyes. Soc Neurosci 2000;26:1075.

Seidemann E, Arieli A, Grinvald A, Slovin H. Dynamics of depolarization and hyperpolarization in the frontal cortex and saccade goal. Science 2002;295:862–5.

Sheth BR, Sharma J, Rao SC, Sur M. Orientation maps of subjective contours in visual cortex. Science 1996;274:2110–5.

Shmuel A, Grinvald A. Functional organization for direction of motion and its relationship to orientation maps in cat area 18. J Neurosci 1996;16:6945–64.

Shoham D, Grinvald A. The cortical representation of the hand in macaque and human area S-I: high resolution optical imaging. J Neurosci 2001;21:6820–35.

Shoham D, Hubner M, Grinvald A, Bonhoeffer T. Spatio-temporal frequency domains and their relation to cytochrome oxidase staining in cat visual cortex. Nature 1997;385:529–33.

Shtoyerman E, Arieli A, Grinvald A. Optical imaging of the primary visual cortex in behaving monkeys. Isr J Med Sci Abstr 1995;31:766.

Shtoyerman E, Arieli A, Slovin H, Vanzetta I, Grinvald A. Long term optical imaging and spectroscopy reveal mechanisms underlying the intrinsic signal and stability of cortical maps in V1 of behaving monkeys. J Neurosci 2000;20:8111–21.

Slovin H, Arieli A, Hildesheim R, Grinvald A. Long-term Voltage-sensitive dye imaging in the behaving monkey. Soc Neurosci Abstr 1999;25:784.

Slovin H, Arieli A, Grinvald A. Voltage-sensitive dye imaging reveals that behavioral context affects population activity in early visual cortex. Soc Neurosci Abstr 2000;26:1082.

Sterkin A, Lampl I, Ferster D, Glaser DE, Grinvald A, Arieli A. Exploring cortical synchronization by simultaneous intracellular recording and dye imaging in cat visual cortex. Soc Neurosci Abstr 1999;25:784.

Ts'o DY, Frostig RD, Lieke E, Grinvald A. Functional organization of primate visual cortex revealed by high resolution optical imaging. Science 1990;249:417–20.

Tsodyks M, Kenet T, Grinvald A, Arieli A. Linking spontaneous activity of single cortical neurons and the underlying functional architecture. Science 1999;286:1943–6.

Wang G, Tanaka K, Tanifuji M. Optical imaging of functional organization in the monkey inferotemporal cortex. Science 1996;272:1665–8.

Weliky M, Bosking W, Fitzpatrick D. A systematic map of direction preference in primary visual cortex. Nature 1996;379:725–8.

Womelsdorf T, Eysel UT, Kisvarday ZF. Comparison of orientation maps obtained with different number of stimulus orientations. Neuroimage 2001;13:1131–9.